An extended flamelet-based presumed probability density function for predicting mean concentrations of various species in premixed turbulent flames

Andrei N. Lipatnikov [a,], Vladimir A. Sabelnikov [b,c]*
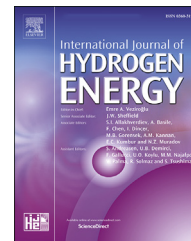
[a] *Department of Mechanics and Maritime Sciences, Chalmers University of Technology, Gothenburg, 41296, Sweden*
[b] *ONERA — the French Aerospace Laboratory, Palaiseau, F-91761, France*
[c] *Central Aerohydrodynamic Institute (TsAGI), Moscow Region, Zhukovsky, 140180, Russian Federation*

HIGHLIGHTS

- A new flamelet-based presumed Probability Density Function approach is developed.
- The flamelet approach quantitatively predicts mean concentrations of radicals.
- The flamelet approach is useful at Karlovitz number larger than 10.

ARTICLE INFO

ABSTRACT

Direct Numerical Simulation (DNS) data obtained by Dave and Chaudhuri (2020) from a lean, complex-chemistry, hydrogen-air flame associated with the thin-reaction-zone regime of premixed turbulent burning are analyzed to perform *a priori* assessment of predictive capabilities of the flamelet approach for evaluating mean species concentrations. For this purpose, dependencies of mole fractions and rates of production of various species on a combustion progress variable c, obtained from the laminar flame, are averaged adopting either the actual Probability Density Function (PDF) $P(c)$ extracted from the DNS data or a common presumed β-function PDF. On the one hand, the results quantitatively validate the flamelet approach for the mean mole fractions of all species, including radicals, but only if the actual PDF $P(c)$ is adopted. The use of the β-function PDF yields substantially worse results for the radicals' concentrations. These findings put modeling the PDF $P(c)$ on the forefront of the research agenda. On the other hand, the mean rate of product creation and turbulent burning velocity are poorly predicted even adopting the actual PDF. These results imply that, in order to evaluate the mean species concentrations, the flamelet approach could be coupled with another model that predicts the mean rate and turbulent burning velocity better. Accordingly, the flamelet approach could be implemented as post-processing of numerical data yielded by that model. Based on the aforementioned findings and implications, a new approach to building a presumed PDF is developed. The key features of the approach consist in (i) adopting a re-normalized flamelet PDF for intermediate values of c and (ii) directly using the mean rate of product creation to calibrate the presumed PDF. Capabilities of the newly developed PDF for predicting mean species concentrations are quantitively validated for all species, including radicals.

* *Corresponding author.*
E-mail addresses: lipatn@chalmers.se, lanna616800@gmail.com (A.N. Lipatnikov), sabelnikov@free.fr (V.A. Sabelnikov).

Introduction

To protect the environment and mitigate the threat of global warming, there is a strong need for replacement of engines that utilize chemical energy bound in fossil fuels with highly efficient, flexible, and ultra clean engines capable for utilizing chemical energy bound in renewable carbon-free fuels. Hydrogen is considered to be one of the most attractive carbon-free fuels due to a variety of H_2 production technologies [1–5] and unique characteristics of hydrogen flames, such as a low ignition energy, a wide range of flammability limits, a high laminar burning velocity, etc. [6]. Accordingly, burning of hydrogen in various engines has been attracting significant amount of attention [6–14], thus, making combustion of hydrogen (including emissions from hydrogen flames [15,16]) an important and rapidly growing area of hydrogen energy. These recent developments have been motivating fundamental research into basic characteristics of laminar combustion of hydrogen [17–20] or fuel blends that contain H_2 [21–25], turbulent burning of hydrogen [26–30] or such fuel blends [31–37], emissions from hydrogen flames [38–43], as well as explosion of hydrogen-air mixtures [44–46].

To increase an impact of the fundamental science on applied research into future ultra-clean and highly efficient engines that burn hydrogen, there is a strong need for development of Computational Fluid Dynamics (CFD) models that (i) allow for complex (and fuel-specific) chemistry of turbulent combustion, and (ii) are capable for predicting mean concentrations of various (not only major reactants and products, but also radicals such as O, OH, H, etc.) species in a turbulent premixed flame under a wide range of conditions. Accordingly, over the past two decades, several approaches, e.g. a transport equation for a Probability Density Function (PDF) [47,48], thickened flame model [49], or flamelet concept [50] coupled with a presumed PDF [51–54], were advanced for predicting concentrations of various species in turbulent flames. In particular, the flamelet concept coupled with a presumed PDF is implemented into major commercial CFD codes and is widely used in applied research, e.g. see Table 4 in Ref. [55]. Such an approach is also in the focus of fundamental studies [56–82] and is supported by recent experimental and Direct Numerical Simulation (DNS) data that, as reviewed elsewhere [83,84], indicate that the domain of validity of the flamelet concept is significantly wider than earlier expected.

The flamelet concept consists in adapting results (the so-called flamelet library) of numerical simulations of a set of laminar premixed flames, performed by invoking a sufficiently detailed model of molecular transport and a sufficiently detailed chemical mechanism. By adopting Flamelet Prolongation of Intrinsic Low-Dimensional Manifolds (FPI) [85] or Flamelet Generation Manifolds (FGM) [86] techniques, a flamelet library is often stored in a form of dependencies of temperature $T_L(\xi)$, density $\rho_L(\xi)$, mole (or mass) fractions $X_{n,L}(\xi)$ and rates $W_{n,L}(\xi)$ of consumption/production of $n = 1, \ldots, N$ species on a set ξ of independent variables. The set ξ may consist of a single combustion progress variable c, which varies from zero in fresh reactants to unity in equilibrium combustion products, but may also involve mixture fraction in the case of partially premixed combustion, mixture enthalpy in the case of non-adiabatic flame, pressure in the case of non-isobaric burning (e.g., in a piston engine), stretch rate in highly turbulent flames, etc. Henceforth, we restrict ourselves to the basic case of a single independent scalar variable c.

To adapt a flamelet library in a Reynolds Averaged Navier-Stokes (RANS) or Large Eddy Simulation (LES) study of turbulent burning, the library should be coupled with a model of the influence of turbulence on combustion. Such a coupling is commonly implemented (i) using the following[1] RANS equations

$$\overline{\mathbf{W}}(\mathbf{x}, t) = \int_0^1 \mathbf{W}_L(c) P(c, \mathbf{x}, t) dc, \tag{1}$$

$$\overline{\mathbf{X}}(\mathbf{x}, t) = \int_0^1 \mathbf{X}_L(c) P(c, \mathbf{x}, t) dc, \tag{2}$$

$$\overline{T}(\mathbf{x}, t) = \int_0^1 T_L(c) P(c, \mathbf{x}, t) dc, \tag{3}$$

$$\overline{\rho}(\mathbf{x}, t) = \int_0^1 \rho(c) P(c, \mathbf{x}, t) dc \tag{4}$$

(or basically similar LES equations, which are not written for brevity) for mean production/consumption rates, mole fractions, temperature, and density, respectively, and (ii) invoking a presumed PDF $P(c, \mathbf{x}, t)$. Here, $\mathbf{W}$ and $\mathbf{X}$ are N-dimensional vector-functions that encompass reaction rates W_n and mole fractions X_n, respectively, for $1 \leq n \leq N$ species.

As reviewed elsewhere [87,88], the presumed PDF is commonly modeled by (i) assuming its general shape, which depends on a few unknown parameters, and (ii) evaluating these parameters by comparing the first two moments of the $c(\mathbf{x}, t)$-field, calculated using the PDF, with the moments obtained by solving their transport equations. The PDF shape is

---

[1] In applications, such equations are commonly adapted for the mass-weighted quantities and PDF. Here, conventional mean quantities and PDF are addressed for simplicity, and because the issues and solutions discussed in the following are basically similar for conventional and mass-weighted quantities.

presumed adopting a sum of Dirac delta functions [52,56,58,63] or combinations of Dirac delta functions and a flamelet PDF [53,54,61,66,73,78], but the β-function PDF $P_\beta(c, \mathbf{x}, t)$ [51] is most widely accepted [53,57,59,60,62,64,65,67–72,74–77,79–82], because its shape is very flexible and, depending on the magnitudes of the afore-mentioned moments, $P_\beta(c, \mathbf{x}, t)$ can vary from a quasi-bi-modal PDF associated with the flamelet regime of premixed turbulent combustion [89] to a quasi-Gaussian PDF associated with extreme turbulence.

Despite the wide use of the flamelet concept jointly with a presumed PDF, such an approach definitely requires better validation and further development. On the one hand, recent simulations aimed at *a posteriori* assessment of the approach have showed its limited capabilities for predicting mean concentrations of intermediate species [59,62,65,70,71,75,76,80,81]. On the other hand, these results are not sufficient to draw the negative conclusion regarding all constituents of the discussed approach. For instance, predictive capabilities of Eq. (1), Eqs. (2)–(4), and a presumed PDF can be significantly different, as will be discussed later. Moreover, substantial disagreement between simulated and measured (or DNS) data, observed in the papers cited above, could stem not only from eventual limitations of the flamelet concept and/or the invoked PDF, but also from limitations of other models invoked in *a posteriori* study. For instance, as reviewed elsewhere [90,91], capabilities of available models for pre-dicting thermal expansion effects in turbulent flames are still very limited and such limitations could contribute to the discussed disagreement.

Therefore, there is still need for *a priory* study that will allow researchers to assess predictive capabilities of Eq. (1), Eqs. (2)–(4), and/or presumed PDFs not only jointly, but also separately. However, *a priory* quantitative assessment of Eqs. (1)–(4) and a presumed PDF have yet been very limited: the presumed β-PDF was quantitatively compared with DNS data by Donini et al. [72], whereas Lapointe and Blanquart [79] explored Eq. (1) for a single rate $\overline{W}_c$, i.e. the source term in the transport equation for the mean combustion progress variable.

The present paper reports results of a study originally conceived with a view to fill the discussed knowledge gap by analyzing recent DNS data [92] in order to perform *a priory* quantitative assessment of Eq. (1), Eqs. (2)–(4), and the pre-sumed β-PDF for various species. It is worth stressing that the work is not limited to exploring these three submodels alto-gether but aims also at testing each submodel separately. The point is that the flamelet concept yielding Eqs. (1)–(4) and the presumed PDF approach are based on different reasoning. Therefore, Eqs. (1)–(4) could perform better than the pre-sumed β-PDF or vice versa. Moreover, despite their apparent similarity, Eqs. (1) and (2) aim at solving basically different problems, i.e., prediction of the mean rate of product creation $\overline{W}_c$ and evaluation of the mean mole fractions of various species. Accordingly, hypotheses and models developed to solve the former problem, which was also attacked in many studies that did not invoke Eq. (1), may differ significantly from hypotheses and models developed to solve the latter problem. Therefore, predictive capabilities of Eqs. (1)–(4) may

be significantly different, see Section A priori assessment of conventional presumed PDF approach and its three constituents.

As will be discussed later, results of the present study did quantitatively validate Eqs. (2)–(4) but supported neither Eq. (1) nor the presumed β-PDF. The latter finding called for advancing the presumed PDF approach by developing a better model of $P(c)$. Therefore, the focus of the study was extended, and another major goal was pursued. Thus, the present work aims not only at assessing Eqs. (1)–(4) and the presumed β-PDF, but also at developing and quantitatively validating a new presumed PDF model.

Moreover, the present study compares different choices of the combustion progress variables.

The structure of the paper is as follows. In the next section, the DNS attributes [92] are briefly reported. Results of *a priory* quantitative assessment of Eq. (1), Eqs. (2)–(4), and the pre-sumed β-PDF are discussed in the third section. A new flamelet-based presumed PDF approach is developed in the fourth section, followed by conclusions.

DNS attributes

The DNS data [92] were computed adapting the Pencil code [93], with the simulation attributes being similar to the attri-butes of earlier simulations performed by the same group and discussed in detail elsewhere [94]. Accordingly, we will restrict ourselves to a brief summary of these attributes.

Both studies [92,94] dealt with statistically 1D, planar pre-mixed flames that propagated along the x-axis in a parallele-piped ($19.18 \times 4.8 \times 4.8$ mm) discretized using a uniform mesh of $960 \times 240 \times 240$ nodes. The periodic boundary conditions were set on the transverse sides and Navier-Stokes Charac-teristic Boundary Conditions [95] were set at the inlet and outlet.

At $t = 0$, a planar laminar flame (H_2-air mixture with the equivalence ratio $\Phi = 0.81$ at 310 K, the laminar flame speed $S_L = 1.84$ m/s and thickness $\delta_L = (T_b - T_u)/\max|\nabla T| = 0.36$ mm) was embedded into the computational domain at $x = x_0$. Subsequently, the 3D continuity, Navier-Stokes, species and energy transport equations were numerically solved using a detailed reaction mechanism (9 species, 21 reactions) by Li et al. [96].

Homogeneous isotropic turbulence was pre-generated using large-scale forcing in a cube with the periodic bound-ary conditions and was evolved until a statistically stationary state was reached. During combustion simulations, the tur-bulence entered the computational domain through the inlet boundary and decayed in the direction of the mean flow. The sole difference between the earlier [94] and recent [92] DNSs consisted of the inlet turbulence characteristics. In the pre-sent case [92], the rms velocity $u' = 6.7$ m/s, an integral length scale $L = 3.1$ mm, an integral time scale $\tau_t = L/u' = 0.46$ ms, turbulent Reynolds number $Re_t = u'L/\nu_u = 950$, Kolmogorov length scale $\eta = (\nu_u^3/\varepsilon)^{1/4} = 0.018$ mm, Kolmogorov time scale $\tau_\eta = (\nu_u/\varepsilon)^{1/2} = 0.015$ ms, Damköhler number $Da = \tau_t/\tau_f = 2.35$, and Karlovitz number $Ka = \tau_f/\tau_\eta = 13.0$. Here, ν is the kinematic viscosity of the mixture; $\varepsilon = 2\nu S_{ij}S_{ij}$ is the rate of

dissipation of turbulent kinetic energy, averaged over the cube; $S_{ij} = (\partial u_i /\partial x_j + \partial u_j /\partial x_i)/2$ is the rate-of-strain tensor; $\tau_t = L/u'$ is the eddy-turn-over time; $\tau_f = \delta_L /S_L$ is the laminar-flame time scale; subscript u or b designates unburned or burned mixture, respectively; and the summation convention applies to repeated indexes.

Four different combustion progress variables were defined as follows: $c_k = (\varphi_k - \varphi_{k,u})/(\varphi_{k,b} - \varphi_{k,u})$. Here, $\varphi_1 = Y_1, \varphi_2 = Y_2$, and $\varphi_3 = Y_3$ are the mass fractions of H_2, O_2, and H_2O, respectively, and $\varphi_4 = T$.

The mean profiles $\overline{q}(\overline{c}_k)$ of various quantities q were evaluated as follows. First, the $q(\mathbf{x}, t)$ and $c_k(\mathbf{x}, t)$-fields were averaged over each transverse plane $x = $ const at each instant t. Second, obtained dependencies of $q(x, t)$ on x were transformed to dependencies of $<q|\overline{\xi} = c_k(t)>$ on a sample variable $\overline{\xi}$ using the averaged profiles of $c_k(x, t)$ divided in 101 intervals, i.e. a transverse plane $x = $ const contributed to the value of $<q|\overline{\xi}_j = c_k(t)>$ provided that $\left| c_k(x, t) - \overline{\xi}_j \right| < 0.005$ with $\overline{\xi}_j = 0.01j$ and $j = 0, ..., 100$. Third, the profiles of $<q|\overline{\xi}_j = c_k(t)>$ were averaged over various instants (54 snapshots stored each 5 μs, 1.401 ms $\leq t \leq$ 1.566 ms), thus, yielding $\overline{q}(\overline{c}_k)$ reported in the following.

To examine Eqs. (1)–(4), PDFs $P_k(\xi, x, t)$ were sampled from grid points characterized by $\left| c_k(\mathbf{x}, t) - \xi_j \right| < 0.005$ for each transverse plane $x = $ const at each instant t. Here, $\xi_j = j/J$ with $j = 0, ..., J$ is a sample variable for the instantaneous $c_k(\mathbf{x}, t)$-fields and $J = 100$ if the opposite is not stated. Subsequently, the instantaneous PDFs were transformed to $P_k(\xi, \overline{\xi}, t)$, as discussed earlier, and were averaged over all instants. Finally, the time-averaged PDFs $P_k(\xi, \overline{c}_k)$ were substituted into Eqs. (1)–(4) to evaluate $\overline{\mathbf{W}}(\overline{c}_k)$, $\overline{\mathbf{X}}(\overline{c}_k)$, $\overline{T}(\overline{c}_k)$, and $\overline{\rho}(\overline{c}_k)$.

The presumed β-function PDFs $P_{\beta,k}(\xi, \overline{c}_k)$ were modeled as follows [51,53].

$$P_{\beta,k}(\xi, \overline{c}_k) = \frac{\Gamma(a+b)}{\Gamma(a)\Gamma(b)}\xi^{a-1}(1-\xi)^{b-1}, \qquad (5)$$

$$a = \overline{c}_k\left(\frac{1}{g_k} - 1\right), \qquad b = (1-\overline{c}_k)\left(\frac{1}{g_k} - 1\right) \qquad (6)$$

by extracting the profiles of $\overline{c_k^2}(\overline{c}_k)$ from the DNS data, as discussed earlier. Here, $\Gamma(a) = \int_0^\infty \zeta^{a-1} e^{-\zeta} d\zeta$ is the gamma function, and $g_k = (\overline{c_k^2} - \overline{c}_k^2)/[\overline{c}_k(1-\overline{c}_k)]$ is the segregation factor. Subsequently, the PDFs $P_{\beta,k}(\xi, \overline{c}_k)$ were applied to average $\mathbf{W}_L(c_k), \mathbf{X}_L(c_k), T_L(c_k)$, and $\rho_L(c_k)$ using Eqs. (1)–(4).

Results and discussion

A priori assessment of conventional presumed PDF approach and its three constituents

Figs. 1 and 2 quantitatively validate Eqs. (3) and (4), respectively, for the fuel-based $c_F \equiv c_1$, product-based c_3, temperature-based c_4 and both for the actual PDF and for the β-function PDFs. The use of the oxygen-based c_2 jointly with the β-function PDF $P_{\beta,2}(\xi, \overline{c}_2)$ results in significantly underestimating the mean density, see dotted line in Fig. 2b. This underestimation

is associated with non-monotonous variation of the mole fraction of O_2 in the laminar flame, as will be discussed later.

The left column in Fig. 3 quantitatively validates Eq. (2) for the major reactants, H_2 and O_2, and product H_2O for all four c_k and for both PDFs. However, the mean mole fractions of radicals, see the middle and right columns in Fig. 3, are well predicted only when (i) the fuel-based combustion progress variable is adopted, see Fig. 3b, and (ii) the actual PDF $P_1(\xi, \overline{c}_1)$ is used, cf. dashed and solid lines. The use of other c_k yields worse results for radicals, especially for H. For HO_2, OH, and O, the worst results are obtained for the oxygen-based c_2, see the second row. Recent analysis [97] of DNS data obtained from highly turbulent lean H_2-air flames also indicated that defining c based on H_2 (O_2) was the best (worst, respectively) choice.

Thus, Figs. 1–3 indicate that, while the analyzed case is characterized by $Ka > 10$ and is associated with strong preferential diffusion effects [26], the flamelet library is useful for predicting mean species concentrations provided that the library is properly adopted. The present results, as well as recent experimental and DNS studies reviewed elsewhere [83,84], imply that the domain of the flamelet concept validity is larger than earlier expected.

On the contrary, Fig. 4 indicates that Eq. (1) performs poorly for the mean rate $\overline{W}_c$ for any of the four combustion progress variables. It is of interest to note that, for the temperature-based c_4, the use of $P_{\beta,4}(\xi, \overline{c}_4)$ yields better results, cf. dotted and solid lines in Fig. 4d, than the actual PDF does, see dashed line. This example illustrates that, if Eqs. (1) and (5) are jointly tested, a wrong conclusion regarding their validity could be drawn due to mutual cancellation of two types of errors (limitations of the flamelet library for the reaction rates and a wrong PDF). Therefore, to assess Eqs. (1)–(5) in a solid manner, each of the equation should also be tested separately.

Limitations of the flamelet library for the reaction rates are also indicated in Fig. 5, which reports evolution of turbulent burning velocities evaluated as follows

$$U_{T,k}(t) = \frac{M_k}{\rho_u (Y_{k,b} - Y_{k,u})} \int_{-\infty}^{\infty} W_k(x, t) dx \qquad (7)$$
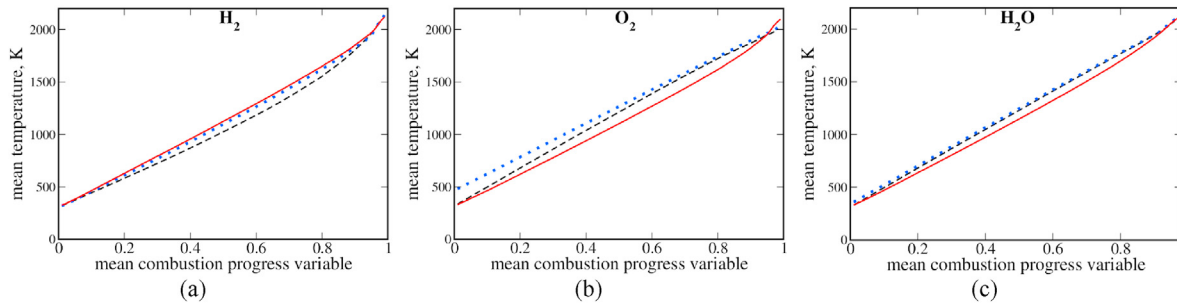
for the species-based combustion progress variables c_1 (H_2), c_2 (O_2), and c_3 (H_2O), or

$$U_{T,4}(t) = \frac{1}{\rho_u(T_b - T_u)} \int_{-\infty}^{\infty} W_4(x, t) dx \qquad (8)$$

for the temperature-based combustion progress variable c_4. Here, M_k is the molecular weight of species k. For each c_k, the actual $U_{T,k}(t)$, see solid lines, differs substantially from $U_{T,k}(t)$ yielded by Eq. (7) or (8) and Eq. (1) with the actual or β-function PDF, see dashed and dotted lines, respectively.

Thus, while both Eq. (1) and Eqs. (2)–(4) stem from the same flamelet concept, Figs. 1–5 clearly show that the former equation performs significantly worse under conditions of the present study. The point is that variations in the mole fractions $\mathbf{X}$, temperature T, or density ρ in a flame are substantially smoother than variations in the rates $\mathbf{W}$ that depend on the temperature in a highly non-linear manner. For instance, Fig. 6 reports dependencies of mole fractions $\mathbf{X}_L(c_F)$ of various

Fig. 1 – **Mean temperature vs. differently defined mean combustion progress variable $\bar{c}_k$. Species used to define c_k are noted in the top of each subfigure. Red solid lines show results extracted directly from the DNS data. Black dashed lines show results obtained by substituting the actual PDFs $P_k(\xi, \bar{c}_k)$ extracted from the DNS data into Eq. (3). Blue dotted lines show results obtained by substituting the β-function PDFs $P_{\beta,k}(\xi, \bar{c}_k)$ into Eq. (3). (For interpretation of the references to color in this figure legend, the reader is referred to the Web version of this article.)**

species and rates $W_L(c_F)$ of their production/consumption on the fuel-based combustion progress variable c_F. These results have been obtained from the unperturbed stationary, planar, 1D laminar flame and have been re-normalized using the peak values of $X_L(c_F)$ or $W_L(c_F)$, respectively. Comparison of Fig. 6a and b indicates significantly smoother variations in $X_{n,L}(c_F)$ when compared to $W_{n,L}(c_F)$ for each species n and a similar trend appears to hold in the studied turbulent flame. Accordingly, eventual errors associated with the flamelet concept, i.e. reduction of $X(x, t)$ and $W(x, t)$ to $X_L[c(x, t)]$ and $W_L[c(x, t)]$, respectively, and eventual errors in modeling the PDF $P(c)$ could result in significantly larger errors when averaging the non-linear rates W when compared to averaging the mole fractions. X.

Implications for modeling

Since Figs. 1–5 indicate that predictive capabilities of Eqs. (2)–(4) are significantly better when compared to Eq. (1), the mean mole fractions of various species, the mean temperature and the mean density can be evaluated by adapting Eqs. (2)–(4) independently of Eq. (1), e.g., by invoking a single-step-chemistry model, which yields a closure relation for the mean rate $\overline{W}_c$ and performs better than Eq. (1). In such a case, $\overline{X}$, $\overline{T}$,
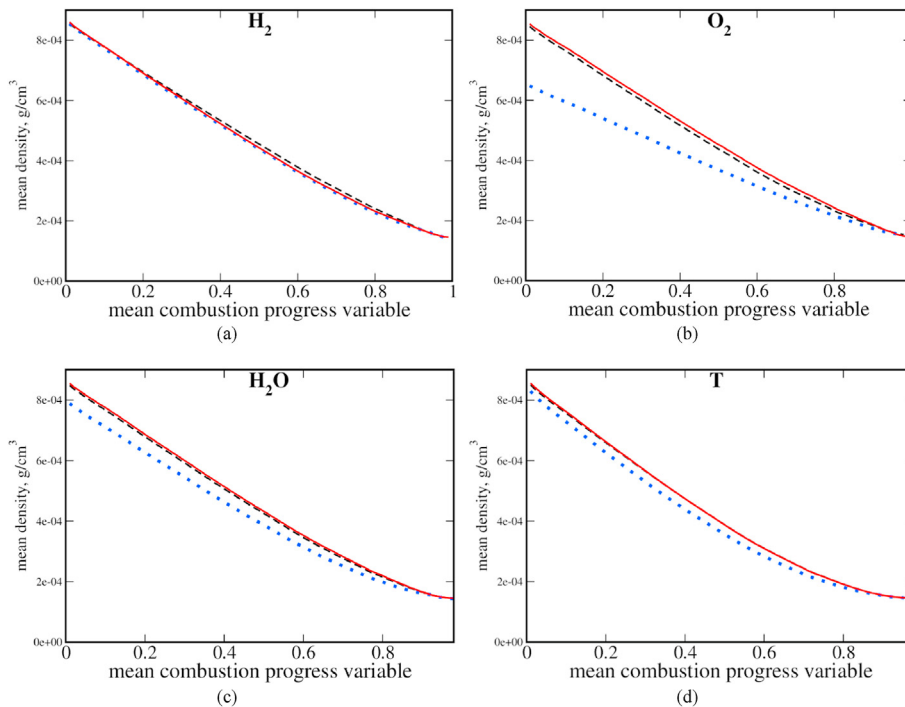
Fig. 2 – **Mean density vs. $\bar{c}_k$. Legends are explained in caption to Fig. 1.**
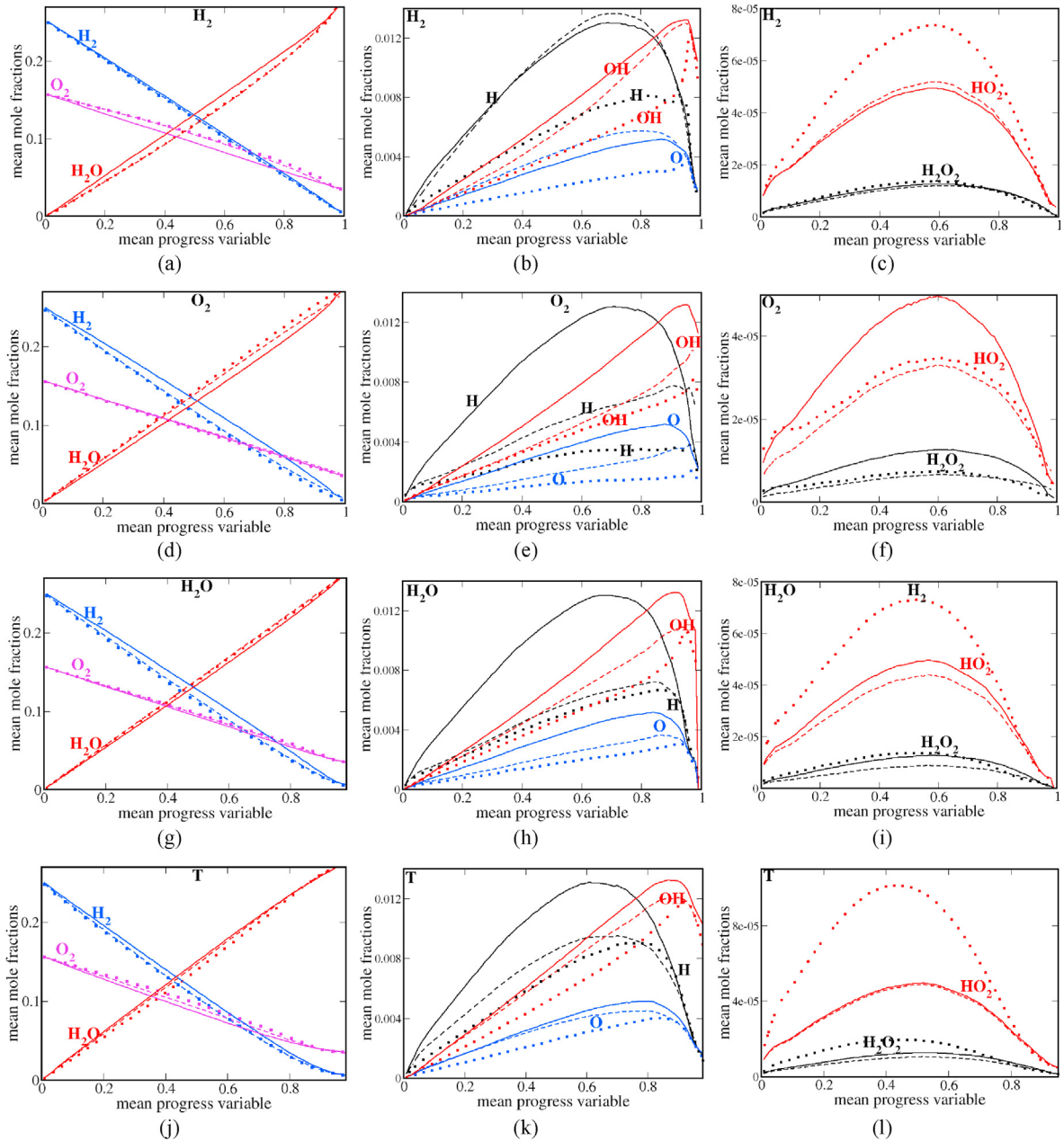
Fig. 3 – **Mean mole fractions of various species noted near relevant curves vs. $\bar{c}_k$. Quantities used to define c_k are specified in the top of each subfigure. Solid lines show results extracted directly from the DNS data. Dashed lines show results obtained by substituting the actual PDFs $P_k(\xi, \bar{c}_k)$ extracted from the DNS data into Eq. (2). Dotted lines show results obtained by substituting the β-function PDFs $P_{\beta,k}(\xi, \bar{c}_k)$ into Eq. (2).**

and $\bar{\rho}$ can be calculated at a post-processing stage after computations of the mean flame speed, thickness, and structure.

Discussion of such a closure relation for $\overline{W}_c$ is beyond the scope of the present work and the interested reader is referred to Refs. [88,89,98–102]. Here, we restrict ourselves to noting that predictive capabilities of simple single-step-chemistry models should not be underestimated. Indeed, first, as hypothesized by Prudnikov [103], reviewed elsewhere [88,98], and supported by more recent experimental data [104,105],

various premixed turbulent flames have the same mean structure, i.e., variations of the Reynolds-averaged $\bar{c}$ along the normal to a mean flame surface are well approximated by the complementary error function if the distance is normalized with the mean flame brush thickness. Single-step-chemistry models can predict this fundamental feature of premixed turbulent combustion [88,98,106–108], whereas any effect of combustion chemistry on the mean flame structure has not yet been revealed.
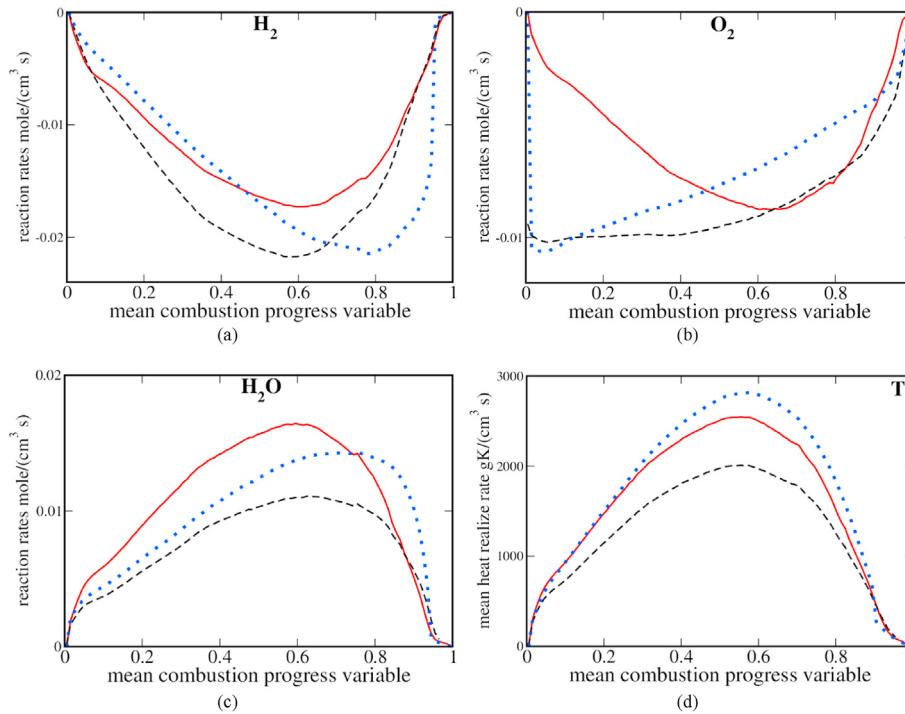
Fig. 4 – Mean rates of (a) fuel consumption, (b) oxygen consumption, (c) water production, or (d) heat release vs. fuel, oxygen, water, or temperature-based combustion progress variable, respectively. Red solid lines show the rates extracted directly from the DNS data. Black dashed lines show the rates calculated by substituting the actual PDFs $P_k(\xi, \bar{c}_k)$ extracted from the DNS data into Eq. (1). Blue dotted lines show the rates calculated by substituting the β-function PDFs $P_{\beta,k}(\xi, \bar{c}_k)$ into Eq. (1). (For interpretation of the references to color in this figure legend, the reader is referred to the Web version of this article.)
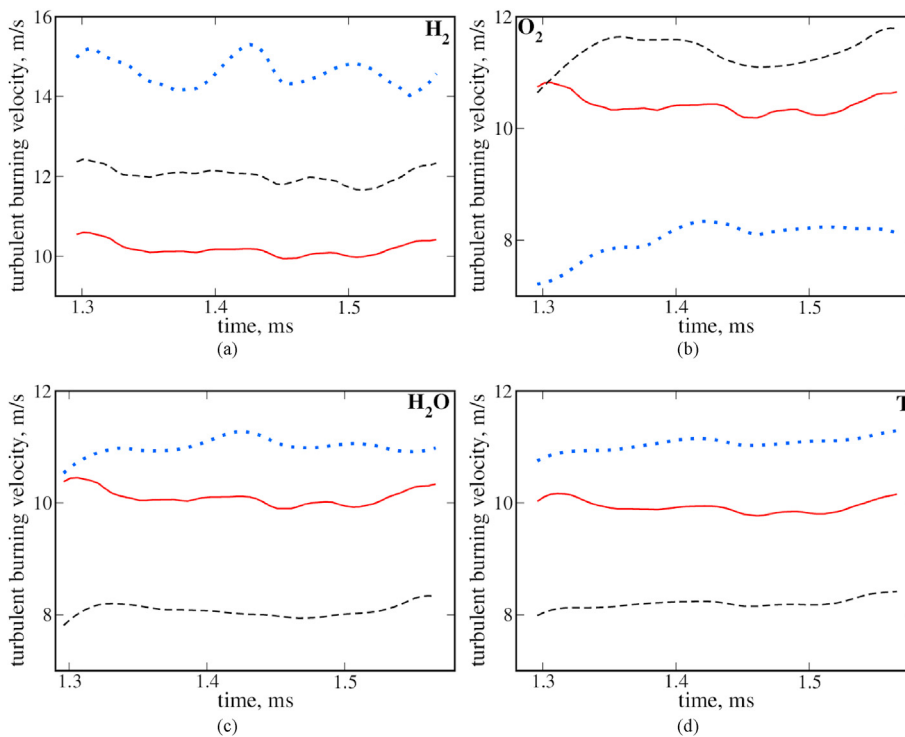
Fig. 5 – Evolution of turbulent burning velocities calculated for (a) fuel, (b) oxygen, (c) water, and (d) temperature-based combustion progress variables. Legends are explained in caption to Fig. 4.
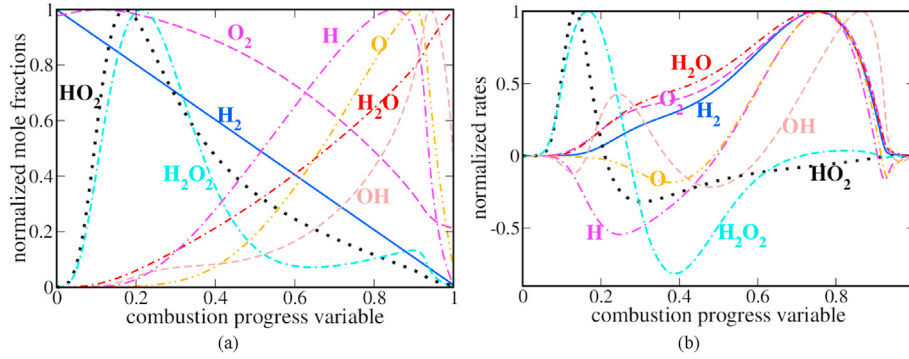
Fig. 6 − **Structure of the unperturbed laminar flame. (a) Mole fractions and (b) rates of production/consumption of various species vs. the fuel-based combustion progress variable c_F. Both the mole fractions and the rates are normalized using their maximal (minimal for the negative rate of consumption on the fuel or oxygen) values.**

Second, as hypothesized by Karlovitz et al. [109], reviewed elsewhere [88,98,103] and supported by more recent data [105,110], the growth of mean turbulent flame brush thickness follows the turbulent diffusion law in various experiments. Single-step-chemistry models can predict this fundamental feature of premixed turbulent combustion [88,98,108], whereas any effect of combustion chemistry on the growth of mean turbulent flame brush thickness has not yet been documented.

Third, while some influence of combustion chemistry on turbulent burning velocity is expected due to local quenching of combustion in extreme turbulence, the flamelet concept does not seem to hold under such conditions. As far as less, but still intense turbulence is concerned, single-step-chemistry models can predict turbulent burning velocity and flame speed reasonably well, as reviewed elsewhere [88,98,108]. It also worth stressing that, in recent DNS studies [111,112], a weak influence of combustion chemistry on U_T has been documented at Karlovitz numbers significantly higher than unity.

To apply Eq. (2) at the post-processing stage, not only a closure relation for the mean rate $\overline{W}_c$, but also a PDF $P(c)$ are required and modeling the PDF still challenges the combustion community. The issue could be addressed by developing approaches that deal with a transport equation for the PDF [47,48]. This research direction appears to be prioritized from the fundamental perspective and the present results provide additional motivation for such investigations.

Alternatively, from the application perspective, the presumed PDF approach could be improved, as the use of the β-function PDF has not allowed us to predict the mean concentrations of radicals, see Fig. 3. This request is responded in the rest of the present paper by taking the following opportunity, which has yet been overlooked. The opportunity stems from the proposed combination of the flamelet Eqs. (2)−(4) with an independent closure relation for the mean rate $\overline{W}_c$. Indeed, if Eq. (1) is not used to close $\overline{W}_c$, but another model of $\overline{W}_c$ is invoked, the presumed PDF could involve one more unknown parameter, because the following three equations

$$1 = \int_0^1 P(c,\mathbf{x},t)dc, \tag{9}$$

$$\overline{c}(\mathbf{x},t) = \int_0^1 cP(c,\mathbf{x},t)dc, \tag{10}$$

$$\overline{c^2}(\mathbf{x},t) = \int_0^1 c^2 P(c,\mathbf{x},t)dc, \tag{11}$$

which (or their mass-weighted counterparts) are typically adopted to evaluate parameters of a common presumed PDF $P(c,\mathbf{x},t)$, could be supplemented with one more constraint of

$$\overline{W}_c(\mathbf{x},t) = \int_0^1 W_{c,L}(c)P(c,\mathbf{x},t)dc, \tag{12}$$

where the mean rate $\overline{W}_c(\mathbf{x},t)$ is considered to be a known quantity yielded by an advanced model of the influence of turbulence on premixed combustion, as discussed earlier. In the rest of the present paper, $\overline{W}_c$ is extracted from the DNS data.

The use of the extra constraint given by Eq. (12), which is similar to Eq. (1), but aims at modeling the PDF $P(c,\mathbf{x},t)$, rather than the mean rate $\overline{W}_c(\mathbf{x},t)$, offers an opportunity to consider a wider set of presumed PDFs, which may involve four parameters. Alternatively, Eq. (11) could be substituted with Eq. (12). In such a case, the number of the PDF parameters is not increased, but a transport equation for the second moment $\overline{c^2}(\mathbf{x},t)$ could be skipped, thus, allowing us to circumvent modeling [102] of the scalar dissipation rate in that transport equation.

Moreover, since consumption of a fuel is mainly localized to reaction zones, substitution of Eq. (11) with Eq. (12) offers an opportunity to build a PDF that better predicts the probability of finding that zone and, hence, better predicts mean concentrations of various species. The mean rate $\overline{W}_c(\mathbf{x},t)$ is

directly linked with the aforementioned probability, whereas such a link appears to be doubtful for the variance $\overline{c'^2}(\mathbf{x}, t)$ [87,88]. The latter claim is obvious in the Bray-Moss-Libby (BML) limit [113], where the variance is solely controlled by the probabilities of finding unburned reactants and equilibrium combustion products.

New flamelet-based presumed PDFs

The encouraging results obtained in the present work by testing the flamelet Eqs. (2)–(4) suggest that the presumed PDF approach could be substantially advanced using the flamelet PDF $P_L(c) \propto 1/(\delta_L |\nabla c|_L)$ [53,54], but also invoking Eq. (12), as proposed earlier [87,88,114]. Development and assessment of such a new presumed flamelet-based PDF is the subject of the following discussion. Henceforth, we restrict ourselves to results computed by adopting the fuel-based combustion progress variable c_F, because the mean concentrations of the radicals were best predicted using c_F, as discussed earlier. Accordingly, subscript F will often be skipped for brevity in the following. Results obtained for the mean density, temperature, and mole fractions of H_2, O_2, and H_2O will not be reported, because, for these quantities, all presumed PDFs discussed in the following yield comparably good agreement with the raw DNS data.

The choice of the flamelet PDF as a starting point is supported in Fig. 7. Indeed, in a large interval of $\xi_1 < c < \xi_2$, appropriately re-normalized flamelet PDFs $P_L(c) = b/(\delta_L |\nabla c|_L)$ are close to the actual PDFs $P(c)$ extracted directly from the DNS data at various $c(x, t)$, cf. dotted and solid lines, respectively. The re-normalization means that Eq. (9) does not hold, but the factor b is tuned in order to minimize the difference between the flamelet and actual PDFs in an interval of c characterized by $P_L(c) < 2\min\{P_L(c)\}$. Accordingly, the tuned value of b depends on $\bar{c}$. The reasons for the re-normalization will be discussed later. It is worth remembering that the actual PDF has been obtained as follows. First, instantaneous PDFs $P[c, \bar{c}(x, t)]$ have independently been extracted from each snapshot, with the PDF variations along the normal to the mean flame brush being characterized by $\bar{c}(x, t)$. Second, those

PDFs have been averaged over time to yield the actual PDF $P(c, \bar{c})$ whose spatial variations are characterized with $\bar{c}$.

Fig. 7 shows that the boundaries ξ_1 and ξ_2 of an interval where the two PDFs match well depend on $\bar{c}$. In the largest part of the mean flame brush, ξ_1 is small and $\xi_2 \approx 0.9$, see Fig. 7b. Since the fuel consumption in the laminar flame occurs at $c \leq 0.9$, see solid line in Fig. 6b, the flamelet PDF $P_L(c)$ plotted in Fig. 7b appears to fit the actual PDF sufficiently well, as far as averaging $W_{L,c}(c)$ is concerned. Fig. 6a implies that the flamelet PDF $P_L(c)$ may also be applied to evaluate mean mole fractions of HO_2 and H_2O_2, because these mole fractions are small at $c > 0.9$ in the laminar flame. However, $P_L(c)$ seems to be less suitable for averaging the mole fractions of HO_2 and H_2O_2 at the trailing edge of the mean flame brush, because ξ_1 is increased by $\bar{c}$, see Fig. 7c. Moreover, the left boundary of the validity domain for the flamelet PDF, i.e. ξ_1, may be increased by Re_t [115], as will be discussed later. Furthermore, (i) the mole fractions of the radicals H, O, and, especially, OH peak at large c in the laminar flame, see Fig. 6a, and (ii) differences between the actual and flamelet PDFs are well pronounced at $c > 0.9$, especially if the mean $\bar{c}$ is low, cf. Fig. 7a and 7c. Accordingly, the flamelet PDF appears to perform worse for the radicals H, O, and OH. Note that the differences between the two PDFs could in part stem from insufficient statistics sampled at $c(\mathbf{x}, t) \to 1$, because the probability of finding $c(\mathbf{x}, t) = 1$ is low under the DNS conditions.

Fig. 7 elucidates one more issue associated with the flamelet PDF. It grows rapidly at $c \to 0$ or $c \to 1$ and is much larger than the actual PDF in these edge zones. Accordingly, such zones can significantly contribute to the integrals on the RHSs of Eqs. 9–12. Consequently, at least one of these constraints is expected to be violated. For instance, as will be discussed in detail later, if substitution of $P_L(c)$ into Eq. (12) allowed us to satisfy this constraint, Eq. (9) would be violated, i.e., its RHS would be too large. Indeed, the RHS of Eq. (9) is controlled by a large $P_L(c \to 1)$, whereas the RHS of Eq. (12) is controlled by much smaller $P_L(0.1 < c < 0.9)$, because the rate $W_c(c)$ vanishes at large c.

From the physical perspective, the use of the flamelet PDF $P_L(c)$ for small and large c appears to be flawed also. As
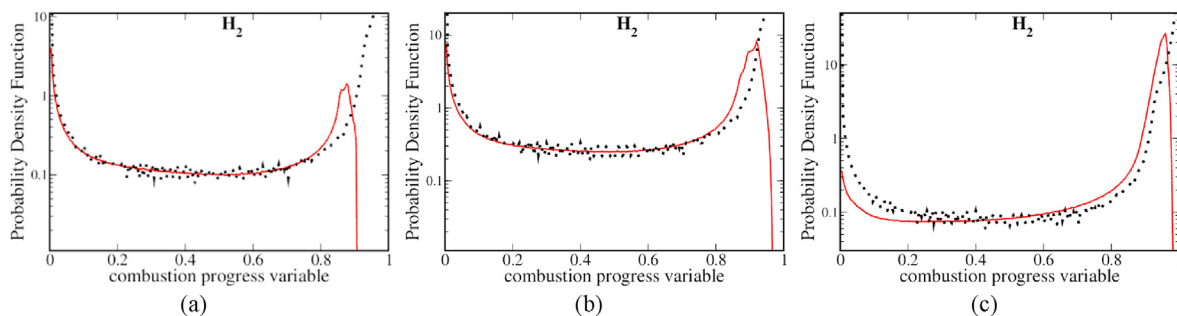
Fig. 7 — Probability Density Functions for the fuel-based combustion progress c_F extracted from the DNS data (red solid lines) and the unperturbed laminar flame (black dotted lines). The former PDFs have been sampled at transverse planes characterized by (a) $\bar{c}_F(x, t) = 0.1$, (b) $\bar{c}_F(x, t) = 0.5$, and (c) $\bar{c}_F(x, t) = 0.9$. The latter PDFs have been re-normalized for each $\bar{c}_F(x)$ to get the best agreement with the DNS data at intermediate values of the sample variable ξ. (For interpretation of the references to color in this figure legend, the reader is referred to the Web version of this article.)

emphasized by Kuznetsov and Sabelnikov [115], at high Reynolds numbers, the local structure of premixed flames at small c is similar to the structure of an inert scalar field, i.e. the gradient ∇c and, hence, the PDF $P(c)$ are controlled by turbulent straining if c is sufficiently small and Re_t is sufficiently high. Indeed, significant perturbations in the local structure and thickness of preheat zones characterized by small c are well documented in highly turbulent flames [83,84]. Similar perturbations are expected to be of substantial importance in the radical-recombination zone [116,117], whose thickness is relatively large, because reactions are relatively slow therein. On the contrary, the local reaction zone appears to be less affected by turbulent eddies, e.g., the zone thicknesses in laminar and turbulent flows are comparable, as reviewed

framework, the parameters α, β, and γ in Eq. (13) and other presumed flamelet-based PDFs discussed in the following are evaluated by adopting Eqs. (9), (10) and (12).

For the PDF presumed by invoking Eq. (13), these three constraints read

$$\alpha + \beta + \gamma = 1, \tag{15}$$

$$\alpha\xi_{\min} + \beta\xi_{\max} + \gamma \int_{\xi_1}^{\xi_2} cP_L(c)dc = \bar{c}, \tag{16}$$

Results reported in the following were obtained by setting

$$\alpha W_{c,L}(\xi_{\min}) + \beta W_{c,L}(\xi_{\max}) + \gamma \int_{\xi_1}^{\xi_2} W_{c,L}(c)P_L(c)dc \cong \gamma \int_{\xi_1}^{\xi_2} W_{c,L}(c)P_L(c)dc = \overline{W}_c. \tag{17}$$

elsewhere [83,84]. Accordingly, adaptation of the flamelet PDF $P_L(c)$ to a bounded interval of $0 < \xi_1 < c < \xi_2 < 1$ seems to be justified better than the use of $P_L(c)$ in the entire interval of $0 \leq c \leq 1$. For these reasons, the PDFs $P_L(c)$ plotted in Fig. 7 are re-normalized and Eq. (9) does not hold for them (if intervals of $c < \xi_1$ and $c > \xi_2$ are not considered, then, integration of the flamelet PDF from zero to unity is not required). We may also note that the flamelet PDFs shown in Fig. 7 vary weakly in wide intervals of c, with the exception of the edge zones. This is consistent with recent experimental and DNS data [83,84] that indicate that reaction zones are thin even in highly turbulent flows. Indeed, if a zone is thin, variations in the actual PDF $P(c)$ are expected to be weak in the zone, see solid lines for $0.2 < c < 0.8$ in Fig. 7, similar to weak variations in $P_L(c)$ in the same interval of c.

Based on the above results and reasoning, the flamelet PDF should solely be applied to a bounded interval of $0 < \xi_1 < c < \xi_2 < 1$, with the PDF being re-normalized to satisfy Eq. (12). To satisfy other constraints, e.g. Eqs. 9 and 10, and, apparently, Eq. (11) if the PDF invokes four parameters, the behavior of $P(c)$ at $c < \xi_1$ and $c > \xi_2$ should also be modeled in a turbulent flame. The simplest presumed PDF that could satisfy all these requirements appears to be as follows

$$P(c) = \alpha\delta(c - \xi_{\min}) + \beta\delta(\xi_{\max} - c) + \gamma H(c - \xi_1)H(\xi_2 - c)P_L(c), \tag{13}$$

where $\delta(x)$ and $H(x)$ are Dirac delta function and Heaviside function, respectively, $0 \leq \xi_{\min} \leq \xi_1$, $\xi_2 \leq \xi_{\max} \leq 1$, and $P_L(c)$ is normalized so that

$$\int_{\xi_1}^{\xi_2} P_L(c)dc = 1. \tag{14}$$

A similar presumed PDF was earlier put forward by Bushe et al. [54,61,66,73], but these authors assumed that $\xi_1 = \xi_{\min}$, $\xi_2 = \xi_{\max}$ and did not adapt Eq. (12) to calibrate the PDF parameters. On the contrary, the use of Eq. (12) is the most important peculiarity of the present approach. Within its

$\xi_{\min} = 0$ and $\xi_2 > 0.9$. Accordingly, the first term on the Left Hand Side (LHS) of Eq. (16) and the first two terms on the LHS of Eq. (17) vanish or are negligibly small.

Fig. 8 shows that, if $\bar{c} < 0.6$ (or $\bar{c} > 0.6$), Eqs. (13–17) with $\xi_{\min} = 0$ and $\xi_{\max} = 1$, see curves 3, predict the mean mole fractions of H and O, see curves[2] 1, better (worse, respectively) than the conventional β-function PDF does, see curves 2. For OH, the two presumed PDFs yield close results if $\bar{c} < 0.4$, but the conventional β-function PDF performs better if $\bar{c} > 0.4$. Thus, substitution of the latter PDF with the considered flamelet-based PDF does not substantially improve predictions of the mean mole fractions of the radicals H, O, and OH. This result is associated with the fact that Eq. (13) does not allow us to model processes localized to the radical-recombination zones characterized by large c, whereas the radical concentrations change drastically in such zones [116,117].

Comparison of curves 3 and 4 in Fig. 8 also emphasizes importance of appropriately modeling contributions from the radical-recombination zones to $\overline{X}_H$, $\overline{X}_O$, and $\overline{X}_{OH}$. The sole difference between the models applied to compute the two curves consists of substitution of $\xi_{\max} = 1$, see curves 3, with $\xi_{\max} = (\xi_2 + 1)/2$, see curves 4. In the latter case, agreement with the mean mole fractions of the radicals, evaluated using the actual PDF, see curves 1, is substantially better. Moreover, Eqs. (13–17) with $\xi_{\min} = 0$ and $\xi_{\max} = (\xi_2 + 1)/2$ perform significantly better than the conventional β-function PDF, see curves 2, for H, O, and OH in the largest part of the mean flame brush with the exception of its trailing edge ($\bar{c} > 0.95$). The improved predictions yielded by Eqs. (13–17) with $\xi_{\min} = 0$ and $\xi_{\max} = (\xi_2 + 1)/2$ imply that a layer around the surface of $c(\mathbf{x}, t) = (\xi_2 + 1)/2$ is sufficiently representative for averaging

---

[2] Curves 1 in Fig. 8 look more scattered than the curves shown in dashed lines in the middle column in Fig. 3, because the PDFs adopted to compute results reported in Fig. 8 have been calculated by dividing the interval of $0 \leq \xi \leq 1$ into a larger number ($J = 250$) of bins.
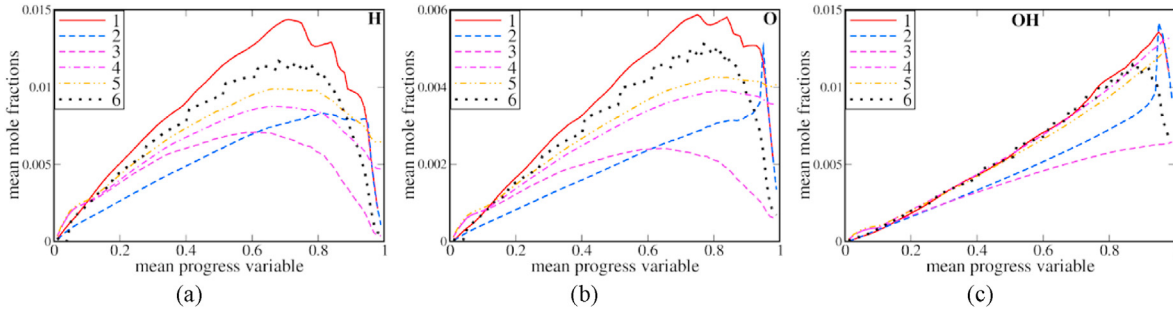
Fig. 8 — Mean mole fractions of (a) H, (b) O, and (c) OH, calculated by substituting various PDFs into Eq. (2), vs. mean fuel-based combustion progress variable. 1 — actual PDF extracted directly from the DNS data; 2 — presumed β-function PDF; 3 — PDF given by Eq. (13) with $\xi_{min} = 0$ and $\xi_{max} = 1$; 4 — PDF given by Eq. (13) with $\xi_{min} = 0$ and $\xi_{max} = (\xi_2 +1)/2$; 5 — PDF given by Eq. (18); 6 — PDF given by Eq. (13) with $\xi_{min} = 0$ and ξ_2 depending on $\bar{c}$. In cases 3–6, $W_{c,L}(c = \xi_1)/\max\{W_{c,L}(c)\} = 0.1$.

the radical concentrations over the recombination zone, because (i) $X_{L,H}(c)$, $X_{L,O}(c)$, and $X_{L,OH}(c)$ peak in the vicinity of $c = (\xi_2 +1)/2$ in the laminar flame under conditions of the present study, see Fig. 6a, and (ii) underestimation of the contribution from the leading half of the zone, i.e., $\xi_2 < c < (\xi_2 +1)/2$, to $\bar{X}_H$, $\bar{X}_O$, and $\bar{X}_{OH}$ is partially counterbalanced by overestimation of the contribution from the trailing half of the zone, i.e., $(\xi_2 +1)/2 < c < 1$. Here, the terms "underestimation" and "overestimation" are used, because the actual PDF is larger (smaller) than the flamelet-based PDF in the leading (trailing, respectively) halves of the zone, see Fig. 7.

To allow for processes localized to the radical-recombination zones, the following simple flamelet-based presumed PDF

$$P(c) = \alpha\delta(c) + \beta H(c - \xi_2)H(1 - c) + \gamma H(c - \xi_1)H(\xi_2 - c)P_L(c), \quad (18)$$

could also be used. When compared to Eq. (13) with $\xi_{min} = 0$, Eq. (18) adopts a constant PDF in the interval of $\xi_2 < c < 1$ instead of a single Dirac delta function. Eqs. (9), (10), (12), (14) and (18) read

$$\alpha + \beta' + \gamma = 1, \quad (19)$$

$$\beta'\frac{1+\xi_2}{2} + \gamma \int_{\xi_1}^{\xi_2} cP_L(c)dc = \bar{c}, \quad (20)$$

$$\gamma \int_{\xi_1}^{\xi_2} W_{c,L}(c)P_L(c)dc \approx \overline{W}_c. \quad (21)$$

Here, $\beta' \equiv \beta(1 - \xi_2)$ and contribution from the second term on the RHS of Eq. (18) to the mean rate $\overline{W}_c$ is neglected, because $W_{c,L}(c > \xi_2)$ is small for the values of ξ_2 used in the present study, see solid curve in Fig. 6b. Curves 5 in Fig. 8a and b shows that Eqs. (18–21) predict $\bar{X}_H$ and $\bar{X}_O$ substantially better than the three other PDFs discussed earlier do. For $\bar{X}_{OH}$, Eqs. (13–17) with $\xi_{min} = 0$ and $\xi_{max} = (\xi_2 +1)/2$ and Eqs. (18–21) perform similarly, but much better than the two other PDFs discussed earlier do.

A common drawback of all the flamelet-based PDFs considered above consists of the lack of a solid criterion for selecting ξ_2. This drawback not only offers a room for tuning, but could also reduce predictive capabilities of the approach, because selection of ξ_2 is not a trivial task. To demonstrate
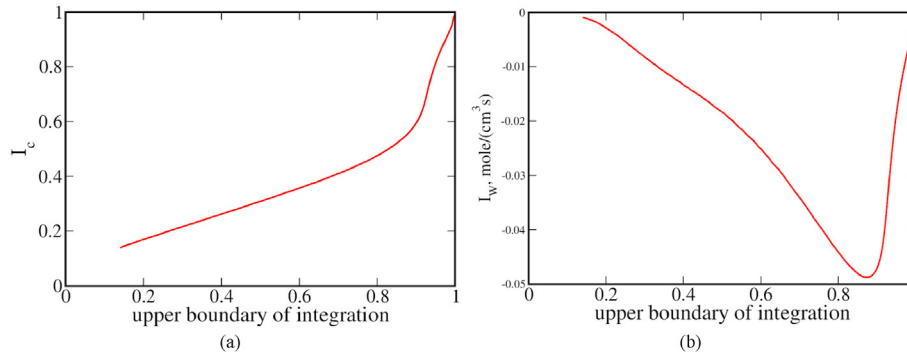
Fig. 9 — Dependencies of integrals (a) $I_c(\xi_1, \xi_2)$ and (b) $I_{W,F}(\xi_1, \xi_2)$ on ξ_2, with $W_{c,L}(c = \xi_1)/\max\{W_{c,L}(c)\} = 0.01$.
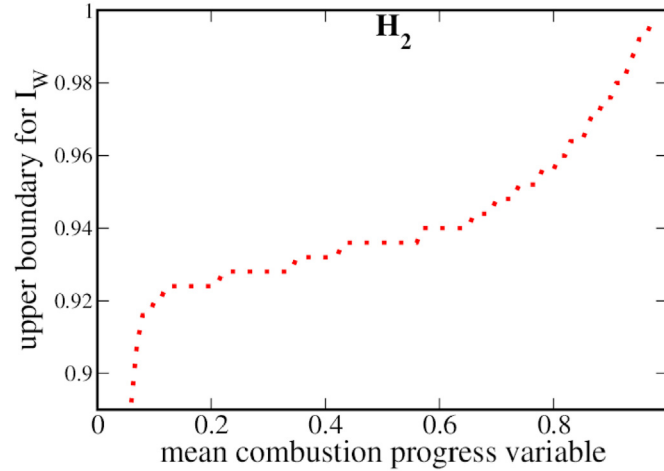
Fig. 10 – Dependence of the optimal ξ_2 on the mean value $\bar{c}_F$ of the fuel-based combustion progress variable.

importance of the appropriate choice of ξ_2, Fig. 9 shows dependencies of the following two integrals

$$I_c(\xi_1,\xi_2) \equiv \int_{\xi_1}^{\xi_2} cP_L(c)dc, \qquad (22)$$

$$I_W(\xi_1,\xi_2) \equiv \int_{\xi_1}^{\xi_2} W_{c,L}(c)P_L(c)dc \qquad (23)$$

on ξ_2 (note that Fig. 9b reports results $I_{W,F}(\xi_1,\xi_2)$ of integration of the negative rate of production of the fuel). These results have been calculated by setting ξ_1 so that $W_{c,L}(c = \xi_1)/\max\{W_{c,L}(c)\} = 0.01$, but the integrals $I_c(\xi_1,\xi_2)$ and, especially, $I_W(\xi_1,\xi_2)$ depend weakly on ξ_1 if it is sufficiently small.

A rapid increase in $I_c(\xi_1,\xi_2)$ when $\xi_2 \rightarrow 1$, see Fig. 9a, results from a sharp increase in $P_L(c \rightarrow 1)$. A decrease in the magnitude $|I_{W,F}(\xi_1,\xi_2)|$ at large ξ_2 is explained as follows. If ξ_2 is increased by retaining the same $P_L(c)$, an integral of $\int_{\xi_1}^{\xi_2} P_L(c)dc$ is significantly increased due to integration of a large $P_L(c)$ over the added interval of c. However, this integral should be equal to unity due to the normalization constraint given by Eq. (14). Consequently, the PDF $P_L(c) = b/(\delta_L|\nabla c|_L)$ should be re-normalized, i.e. b should be decreased with increasing ξ_2. The decrease in b results in decreasing $P_L(c)$ and, hence, $W_{c,L}(c)P_L(c)$ in the reaction zone, where the rate $W_{c,L}(c)$ is high. On the contrary, the extension of the integration domain to larger c has a minor direct effect on $I_W(\xi_1,\xi_2)$, because the rate $W_{c,L}(c)$ is too low in the added domain. Accordingly, the indirect effect, i.e. the decrease in b, required to satisfy Eq. (14) when increasing ξ_2, dominates and the integral $I_W(\xi_1,\xi_2)$ is decreased at large ξ_2.

Fig. 9 indicates that the use of Eqs. (13) and (14) requires an appropriate pre-selection of ξ_2. For instance, if $\bar{c}$ is too small, substitution of γ given by Eq. (17) or (21) into Eq. (16) or (20), respectively, could yield $\gamma I_c(\xi_1,\xi_2) > \bar{c}$ for certain ξ_2, thus, requiring negative α or β. Moreover, since $\gamma \leq 1$ due to Eq. (15)

or (19), Eq. (17) or (21) with ξ_2 considered to be independent of $\bar{c}$ can be satisfied only if $|I_W(\xi_1,\xi_2)| \geq \max\{\overline{W}_c(\bar{c})\}$ and this constraint has been adopted when calculating results plotted in curves 3–5 in Fig. 8. Otherwise, $|I_W(\xi_1,\xi_2)|$ can be too small if ξ_2 is too large, see Fig. 9b. In such a case, Eqs. (15) and (17) or (19) and (21) require $\gamma \leq 1$ and $\gamma > 1$, respectively. However, for $\bar{c}$ associated with $\overline{W}_c(\bar{c}) < \max\{\overline{W}_c(\bar{c})\}$, lower values of $I_W(\xi_1,\xi_2)$ can be consistent with Eqs. (12) and (17), or (21). Accordingly, a larger ξ_2 may be set to extend an interval that the flamelet PDF is applied to. This extension is beneficial, because (i) the flamelet and actual PDFs match in a wide range of c in Fig. 7 and (ii) the former PDF is based on physical reasoning, whereas the second term on the RHS of Eq. (13) or (18) is sufficiently arbitrary. An increase in ξ_2 results in increasing (decreasing) an interval of c that the third (second, respectively) term on the RHS of Eq. (13) or (18) is applied to. Accordingly, the third and physically sound (second and arbitrary) term plays a more (less, respectively) important role when ξ_2 is increased. Thus, ξ_2 can and should vary with $\bar{c}$.

Accordingly, the following unified algorithm is proposed to build the flamelet-based presumed PDF by adopting Eqs. (13–17) in the simplest case of $\xi_{min} = 0$ and $\xi_{max} = 1$. First, the integrals $I_c(\xi_1,\xi_2)$ and $I_W(\xi_1,\xi_2)$ are pre-calculated for various ξ_2 by processing data obtained in simulations of the unperturbed complex-chemistry laminar flame. Second, for each $\bar{c}$, the product of $\gamma I_W(\xi_1,\xi_2)$ is compared with $\overline{W}_c(\bar{c})$ and the largest value of $\xi_{2,i}$ consistent with Eq. (17) is selected. If this value is also consistent with Eqs. (15) and (16), where $0 \leq \alpha \leq 1$, $0 \leq \beta \leq 1$, and $0 \leq \gamma \leq 1$, the mean mole fractions are evaluated using Eq. (2). Otherwise, the next lower value $\xi_{2,i-1}$ is used and the procedure is repeated until all three constraints, i.e. Eqs. (15–17), are satisfied for certain "optimal" $\xi_{2,i-j}$, where $0 \leq j < i$. While there is no guarantee that all these constraints can simultaneously be satisfied, this is so for $\bar{c} \geq 0.06$ in the present study. For lower $\bar{c}$, the algorithm does not seem to be applicable, because the PDF $P(c,\bar{c})$ tends to Dirac delta function $\delta(c)$ as $\bar{c} \rightarrow 0$, the rate $\overline{W}_c(\bar{c} \rightarrow 0) \rightarrow 0$, and the mean concentrations of radicals are very low at small $\bar{c}$. Accordingly, at low $\bar{c}$,
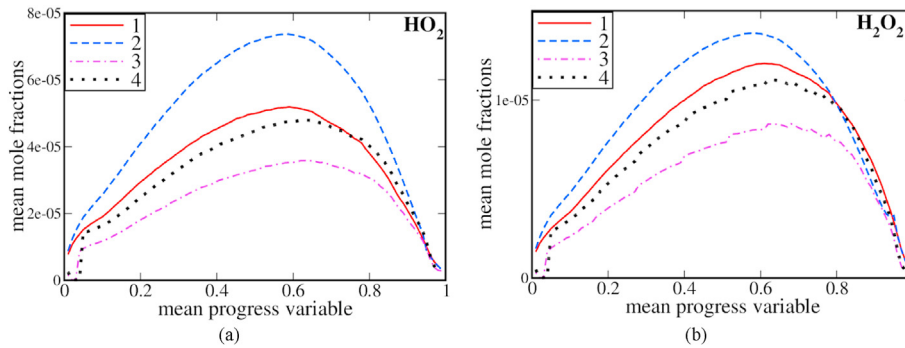
Fig. 11 — Mean mole fractions of (a) HO_2 and (b) H_2O_2, calculated by substituting various PDFs into Eq. (2), vs. mean fuel-based combustion progress variable. 1 — actual PDF extracted directly from the DNS data; 2 — presumed β-function PDF; 3 — PDF given by Eq. (13) with $\xi_{min} = 0$, $\xi_{max} = 1$, and $W_{c,L}(c = \xi_1)/\max\{W_{c,L}(c)\} = 0.1$; 4 — PDF given by Eq. (13) with $\xi_{min} = 0$, $\xi_{max} = 1$, and $W_{c,L}(c = \xi_1)/\max\{W_{c,L}(c)\} = 0.01$.

one can assume that $\beta = 0$ and find two other PDF parameters adopting Eqs. (15) and (16). Then, the algorithm is straightforward and free from tuning (the choice of ξ_1 will be discussed later) provided that the PDF shape is presumed, e.g., Eq. (13) with $\xi_{min} = 0$ and $\xi_{max} = 1$ is invoked.

Results computed by adopting Eqs. (13–17) and the suggested algorithm are shown in curves 6 in Fig. 8. Agreement with the mean mole fractions computed by substituting the actual DNS into Eq. (2) is encouraging for all three radicals. Some scatter of the former results stems from (i) the use of a discrete set of allowed ξ_2 and (ii) a step growth of the optimal $\xi_{2,i-j}$ with $\overline{c}$, see Fig. 10. Note that ξ_1 has been selected based on the constraint of $W_{c,L}(c = \xi_1)/\max\{W_{c,L}(c)\} = \varepsilon$, with almost the same results being obtained for $\varepsilon = 0.1$ and 0.01 under conditions of the present study. It is worth remembering, however, that the use of a larger ε and, hence, a larger ξ_1 may be necessary at higher turbulent Reynolds numbers [115].

While, under conditions of the present study, the value of $\varepsilon \ll 1$ weakly affects $\overline{X}_H(\overline{c})$, $\overline{X}_O(\overline{c})$, and $\overline{X}_{OH}(\overline{c})$ calculated by adapting various extended flamelet-based presumed PDFs discussed above, this value should be sufficiently small in order for these PDFs to predict $\overline{X}_{HO_2}(\overline{c})$ and $\overline{X}_{H_2O_2}(\overline{c})$, cf. curves 3

and 4 in Fig. 11. As suggested in Fig. 6a and confirmed by the present analysis of the DNS data, these results are weakly sensitive to the behavior of the PDFs at large c. Accordingly, solely profiles calculated using the simplest Eq. (13) with $\xi_{min} = 0$ and $\xi_{max} = 1$ are reported in Fig. 11. Comparison of curves 1 and 4 shows that the extended flamelet-based presumed PDF well predicts the mean mole fractions of HO_2 and H_2O_2 provided that ξ_1 is sufficiently small. This PDF performs better than the conventional β-function PDF does, see curves 2.

Finally, predictive capabilities of the developed flamelet-based presumed PDF approach are quantitatively validated in Fig. 12. The dashed lines show results computed by adopting Eqs. (18–21) with $\xi_{min} = 0$, ξ_2 depending on $\overline{c}$, and ξ_1 resulting from the constraint of $W_{c,L}(c = \xi_1)/\max\{W_{c,L}(c)\} = 0.01$. For all intermediate species with the exception of H_2O_2, the approach is clearly superior to the use of the conventional β-function PDF. There is a room for further improvement of the model, e.g., by smoothing variations in ξ_2 with $\overline{c}$ in order to smooth curves shown in dashed lines in Fig. 12a. However, such polishing of the developed approach does not seem to be necessary at this stage of research, because the achieved
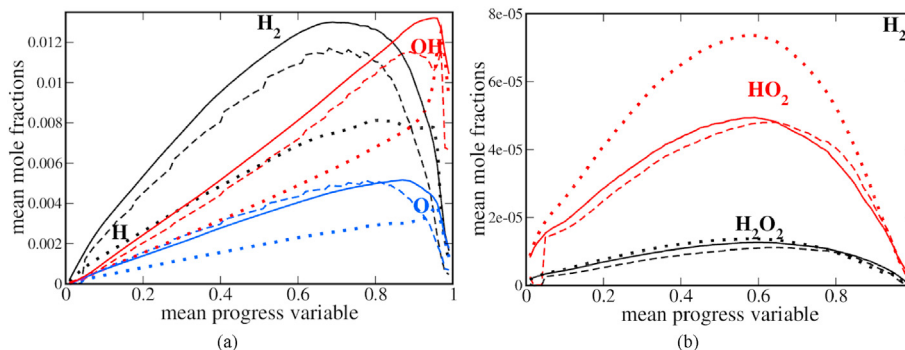
Fig. 12 — Mean mole fractions of intermediate species specified near relevant curves vs. mean fuel-based combustion progress variable. Solid lines show results extracted directly from the DNS data. Dashed lines show results obtained by substituting the PDF given by Eq. (18) with $\xi_{min} = 0$ and ξ_2 depending on $\overline{c}$ into Eq. (2). Dotted lines show results obtained by substituting the conventional β-function PDF into Eq. (2).

agreement between the model and DNS results is already impressive, cf. dashed and solid lines in Fig. 12. Therefore, if the developed approach is adopted in a CFD study, precision of numerical simulations of mean concentrations of various species in a premixed turbulent flame appears to be controlled by other invoked models, e.g., by models of turbulence in premixed flames [90,91].

In other words, Fig. 12 implies that, from the purely application perspective, modeling the PDF $P(c)$ is no longer a bottleneck, at least under conditions of the present study. Assessment of the developed approach at higher Reynolds numbers, higher Karlovitz numbers, for other fuels and species, or/and within the LES framework appear to be more important and interesting tasks for future research. Nevertheless, it is worth remembering that the presumed PDF given by Eq. (13) or (18) invokes a very simple approximation of $P(c)$ at large c. While such simplifications appear to be justified for applications, at least at the present stage of CFD research into complex-chemistry premixed turbulent combustion, these simplifications may be disputed from the fundamental perspective. Therefore, the behavior of $P(c)$ at large c definitely requires further study, e.g., by advancing the transport equation for the PDF. In particular, comparison of results obtained by adapting different PDFs, see Fig. 8, motivates target-directed investigation of $P(c)$ and its transport equation in the radical-recombination zone of complex-chemistry flames. This task is of crucial importance for predicting the mean concentrations of H, O, and OH.

Conclusions

A quantitative *a priori* assessment of the flamelet approach to evaluating the mean density $\bar{\rho}$, the mean temperature $\bar{T}$, the mean mole fractions $\bar{X}_n$ of various species, and the mean source term $\overline{W}_c$ in the transport equation for the mean combustion progress variable $\bar{c}$ has been performed by analysing complex-chemistry DNS data obtained recently by Dave and Chaudhuri [92] from a lean hydrogen-air flame characterized by $u'/S_L = 3.6$ and the Karlovitz number $Ka = 13$. Four different choices of the combustion progress variable have been probed, with the PDF $P(c)$ being either (i) extracted directly from the DNS data or (ii) presumed by invoking the widely-used β-function and adopting the first two moments of the $c(\mathbf{x},t)$-field extracted directly from the DNS data.

The results show that $\bar{\rho}(\bar{c})$, $\bar{T}(\bar{c})$, and $\bar{X}_n(\bar{c})$ for all species (major reactants H_2 and O_2, product H_2O, and radicals H, O, OH, HO_2 and H_2O_2) are well predicted by the flamelet Eqs. (2)–(4) provided that (i) the combustion progress variable is defined using the fuel mass fraction and (ii) the actual PDF extracted directly from the DNS data is substituted into these equations. In line with other recent experimental and DNS data reviewed elsewhere [83,84], this result indicates that the domain of validity of the flamelet concept is substantially

wider than earlier expected. The use of the β-function PDF yields substantially worse results for the radicals. The mean rate $\overline{W}_c$ and turbulent burning velocity based on it are poorly predicted for all probed c even if the actual PDF is substituted into Eq. (1).

These findings imply that, in order to evaluate the mean temperature, density and species concentrations, Eqs. (2)–(4) could be coupled with another closure relation for the mean rate $\overline{W}_c$, whose predictive capabilities are better documented when compared to Eq. (1). In such a case, Eqs. (2)–(4) could be implemented as post-processing of a mean $\bar{c}$-field computed by numerically integrating a single transport equation for the mean combustion progress variable.

Therefore, modeling the PDF $P(c)$ in Eqs. (2)–(4) is put on the forefront of the research agenda. Accordingly, an extended flamelet-based presumed PDF approach has been developed by using the mean rate $\overline{W}_c$ for the PDF calibration. If the rate is extracted from the DNS data, the newly developed approach well predicts mean concentrations of all species (H_2, O_2, H_2O, H, O, OH, HO_2, H_2O_2) without using any tuning parameter.

Declaration of competing interest

The authors declare that they have no known competing financial interests or personal relationships that could have appeared to influence the work reported in this paper.

Acknowledgements

REFERENCES

[1] Yilancia A, Dincer I, Ozturk HK. A review on solar-hydrogen/fuel cell hybrid energy systems for stationary applications. Prog Energy Combust Sci 2009;35:231–44.
[2] Gahleitner G. Hydrogen from renewable electricity: an international review of power-to-gas pilot plants for stationary applications. Int J Hydrogen Energy 2013;38:2039–61.
[3] Hou HJM. Hydrogen energy production using manganese/semiconductor system inspired by photosynthesis. Int J Hydrogen Energy 2017;42:8530–8.
[4] Orfila M, Linares M, Molina R, Botas JÁ, Marugán J, Sanz R. Thermochemical hydrogen production using manganese cobalt spinels as redox materials. Int J Hydrogen Energy 2017;42:13532–43.

[5] Ramalingam S, Rajendiran B, Subramiyan S. Recent advances in the performance of Co-current gasification technology: a review. Int J Hydrogen Energy 2019;45:230–62.

[6] Verhelst S, Wallner T. Hydrogen-fueled internal combustion engines. Prog Energy Combust Sci 2009;35:490–527.

[7] Karim GA. Hydrogen as a spark ignition engine fuel. Int J Hydrogen Energy 2003;28:569–77.

[8] Tian Y, Yang S, Le J, Su T, Tain X. Investigation of combustion and flame stabilization modes in a hydrogen fueled scramjet combustor. Int J Hydrogen Energy 2016;41(42):19218–30.

[9] Haller J, Link T. Thermodynamic concept for an efficient zero-emission combustion of hydrogen and oxygen in stationary internal combustion engines with high power density. Int J Hydrogen Energy 2017;42:27374–87.

[10] Luo QH, Sun BG. Inducing factors and frequency of combustion knock in hydrogen internal combustion engines. Int J Hydrogen Energy 2016;41:16296–305.

[11] Yu X, Li G, Du Y, Guo Z, Shang Z, He F, Shen Q, Li D, Li Y. A comparative study on effects of homogeneous or stratified hydrogen on combustion and emissions of a gasoline/hydrogen SI engine. Int J Hydrogen Energy 2019;44:25974–84.

[12] Yip HL, Srna A, Yuen ACY, Kook S, Taylor RA, Yeoh GH, Medwell PR, Chan QN. A review of hydrogen direct injection for internal combustion engines: towards carbon-free combustion. Appl Sci 2019;9:4842.

[13] Choubey G DY, Huang W, Yan L, Babazadeh H, Pandey KM. Hydrogen fuel in scramjet engines - a brief review. Int J Hydrogen Energy 2020;45:16799–815.

[14] Amell A, Olsen DB, Diaz GJA. Strategies to improve the performance of a spark ignition engine using fuel blends of biogas with natural gas, propane and hydrogen. Int J Hydrogen Energy 2018;43:21592–602.

[15] Deb M, Sastry GRK, Bose PK, Banerjee R. An experimental study on combustion, performance and emission analysis of a single cylinder, 4-stroke DI-diesel engine using hydrogen in dual fuel mode of operation. Int J Hydrogen Energy 2015;40:8586–98.

[16] Banerjee R, Roy S, Bose PK. Hydrogen-EGR synergy as a promising pathway to meet the PM-NOx-BSFC trade-off contingencies of the diesel engine: a comprehensive review. Int J Hydrogen Energy 2015;40:12824–47.

[17] Zamashchikov VV, Alekseev VA, Konnov AA. Laminar burning velocities of rich near-limiting flames of hydrogen. Int J Hydrogen Energy 2014;39:1874–81.

[18] Yakovenko IS, Ivanov MF, Kiverin AD, Melnikova KS. Large-scale flame structures in ultra-lean hydrogen-air mixtures. Int J Hydrogen Energy 2018;43(3):1894–901.

[19] Liu Q, Chen X, Shen Y, Zhang Y. Parameter extraction from spherically expanding flames propagated in hydrogen/air mixtures. Int J Hydrogen Energy 2019;44(2):1227–38.

[20] Gavrikov AI, Golub VV, Mikushkin AY, Petukhov VA, Volodin VV. Lean hydrogen-air premixed flame with heat loss. Int J Hydrogen Energy 2019;44(36):20462–9.

[21] Tahtouh T, Halter F, Mounaïm-Rousselle C. Laminar premixed flame characteristics of hydrogen blended isooctane-air-nitrogen mixtures. Int J Hydrogen Energy 2011;36(1):985–91.

[22] Aravind B, Kishore VR, Mohammad A. Combustion characteristics of the effect of hydrogen addition on LPG-air mixtures. Int J Hydrogen Energy 2015;40:16605–17.

[23] Pan W, Liu D. Effects of hydrogen additions on premixed rich flames of four butanol isomers. Int J Hydrogen Energy 2017;42(6):3833–41.

[24] Varghese RJ, Kumar S. Machine learning model to predict the laminar burning velocities of $H_2/CO/CH_4/CO_2/N_2$/air mixtures at high pressure and temperature conditions. Int J Hydrogen Energy 2020;45(4):3216–32.

[25] Jithin EV, Varghese RJ, Velamati RK. Experimental and numerical investigation on the effect of hydrogen addition and N_2/CO_2 dilution on laminar burning velocity of methane/oxygen mixtures. Int J Hydrogen Energy 2020;45:16838–50.

[26] Lipatnikov AN, Chomiak J. Molecular transport effects on turbulent flame propagation and structure. Prog Energy Combust Sci 2005;31(1):1–74.

[27] Yenerdag B, Minamoto Y, Naka Y, Shimura M, Tanahashi M. Flame propagation and heat transfer characteristics of a hydrogen–air premixed flame in a constant volume vessel. Int J Hydrogen Energy 2016;41(22):9679–89.

[28] Ranga Dinesh Kkj, Shalaby H, Luo KH, van Oijen JA, Thévenin D. High hydrogen content syngas fuel burning in lean premixed spherical flames at elevated pressures: effects of preferential diffusion. Int J Hydrogen Energy 2016;41(40):18231–49.

[29] Lipatnikov AN, Chakraborty N, Sabelnikov VA. Transport equations for reaction rate in laminar and turbulent premixed flames characterized by non-unity Lewis number. Int J Hydrogen Energy 2018;43(45):21060–9.

[30] Minamoto Y, Tanahashi M. Effect of turbulent motions at different length scales on turbulent premixed swirl-stabilised flame topology. Int J Hydrogen Energy 2019;44:22316–27.

[31] Chiu CW, Dong YC, Shy SS. High-pressure hydrogen/carbon monoxide syngas turbulent burning velocities measured at constant turbulent Reynolds numbers. Int J Hydrogen Energy 2012;37(14):10935–46.

[32] Mansouri Z, Aouissi M, Boushaki T. Numerical computations of premixed propane flame in a swirl-stabilized burner: effects of hydrogen enrichment, swirl number and equivalence ratio on flame characteristics. Int J Hydrogen Energy 2016;41(22):9664–78.

[33] Cecere D, Giacomazzi E, Arcidiacono NM, Picchia FR. Direct numerical simulation of high pressure turbulent lean premixed CH_4/H_2-air slot flames. Int J Hydrogen Energy 2018;43(10):5184–98.

[34] Xie Y, Sun ZY. Effects of the external turbulence on centrally-ignited spherical unstable CH_4/H_2/air flames in the constant-volume combustion bomb. Int J Hydrogen Energy 2019;44:20452–61.

[35] Zhang GP, Li GX, Li HM, Jiang YH, Lv JC. Experimental investigation on the self-acceleration of 10%H_2/90%CO/air turbulent expanding premixed flame. Int J Hydrogen Energy 2019;44:24321–30.

[36] Zhang M, Chang M, Wang J, Huang Z. Flame dynamics analysis of highly hydrogen-enrichment premixed turbulent combustion. Int J Hydrogen Energy 2020;45(1):1072–83.

[37] Huang K, Sun ZY, Tian YC, Wang KL. Turbulent combustion evolution of stoichiometric H_2/CH_4/air mixtures within a spherical space. Int J Hydrogen Energy 2020;45:10613–22.

[38] Yilmaz H, Cam O, Tangoz S, Yilmaz I. Effect of different turbulence models on combustion and emission characteristics of hydrogen/air flames. Int J Hydrogen Energy 2017;42(40):25744–55.

[39] Zhu H, Duan J. Research on emission characteristics of hydrogen fuel internal combustion engine based on more detailed mechanism. Int J Hydrogen Energy 2019;44:5592–8.

[40] Bazooyar B, Shariati A, Khosravi-Nikou M, Hashemabadi SH. Numerical analysis of nitrogen oxides in

31177

turbulent lifted H_2/N_2 Cabra jet flame issuing into a vitiated coflow. Int J Hydrogen Energy 2019;44:13932–52.

[41] Iavarone S, Cafiero M, Ferrarotti M, Contino F, Parente A. A multiscale combustion model formulation for NOx predictions in hydrogen enriched jet flames. Int J Hydrogen Energy 2019;44:23436–57.

[42] de Persis S, Idir M, Molet J, Pillier L. Effect of hydrogen addition on NOx formation in high-pressure counter-flow premixed CH_4/air flames. Int J Hydrogen Energy 2019;44:23484–502.

[43] Ali G, Zhang T, Wu W, Zhou Y. Effect of hydrogen addition on NOx formation mechanism and pathways in MILD combustion of H_2-rich low calorific value fuels. Int J Hydrogen Energy 2020;45:9200–10.

[44] Bauwens CRL, Bergthorson JM, Dorefeev SB. Experimental investigation of spherical-flame acceleration in lean hydrogen-air mixtures. Int J Hydrogen Energy 2017;42:7691–7.

[45] Golub VV, Korobov AE, Mikushkin AY, Solntsev OI, Volodin VV. Acceleration of hydrogen/air flames in a cylindrical envelope. Int J Hydrogen Energy 2017;42(17):12724–34.

[46] Makarov D, Hooker P, Kuznetsov M, Molkov V. Deflagrations of localised homogeneous and inhomogeneous hydrogen-air mixtures in enclosures. Int J Hydrogen Energy 2018;43:9848–69.

[47] Haworth DC. Progress in probability density function methods for turbulent reacting flows. Prog Energy Combust Sci 2010;36:168–259.

[48] Pope SB. Small scales, many species and the manifold challenges of turbulent combustion. Proc Combust Inst 2013;34(1):1–31.

[49] Colin O, Ducros F, Veynante D, Poinsot T. A thickened flame model for large eddy simulations of turbulent premixed combustion. Phys Fluids 2000;12:1843–63.

[50] Peters N. Laminar flamelet concepts in turbulent combustion. Proc Combust Inst 1986;21:1231–49.

[51] Peters N. The premixed turbulent flame in the limit of a large activation energy. J Non-Equil Thermod 1982;7:25–38.

[52] Libby PA, Williams FA. Presumed PDF analysis of partially premixed turbulent combustion. Combust Sci Technol 2000;161:359–90.

[53] Bray KNC, Champion M, Libby PA, Swaminathan S. Finite rate chemistry and presumed PDF models for premixed turbulent combustion. Combust Flame 2006;146:665–73.

[54] Jin B, Grout R, Bushe WK. Conditional source-term estimation as a method for chemical closure in premixed turbulent reacting flow. Flow, Turbul Combust 2008;81:563–82.

[55] Gicquel LYM, Staffelbach G, Poinsot T. Large eddy simulations of gaseous flames in gas turbine combustion chambers. Prog Energy Combust Sci 2012;38(6):782–815.

[56] Ribert G, Champion M, Plion P. Modeling a turbulent reactive flow with variable equivalence ratio: application to the calculation of a reactive shear layer. Combust Sci Technol 2004;176:907–23.

[57] Fiorina B, Gicquel O, Vervisch L, Carpentier S, Darabiha N. Premixed turbulent combustion modeling using tabulated detailed chemistry and PDF. Proc Combust Inst 2005;30:867–74.

[58] Robin V, Mura A, Champion M, Degardin O, Renou B, Boukhalfa M. Experimental and numerical analysis of stratified turbulent V-shaped flames. Combust Flame 2008;153:288–315.

[59] Galpin J, Naudin A, Vervisch L, Angelberger C, Colin O, Domingo P. Large-eddy simulation of a fuel-lean premixed turbulent swirl-burner. Combust Flame 2008;155:247–66.

[60] Vreman AW, van Oijen JA, de Goey LPH, Bastiaans RJM. Subgrid scale modeling in large-eddy simulation of turbulent combustion using premixed flamelet chemistry. Flow, Turbul Combust 2009;82:511–35.

[61] Salehi MM, Bushe WK. Presumed PDF modeling for RANS simulation of turbulent premixed flames. Combust Theor Model 2010;4:381–403.

[62] Kolla H, Swaminathan N. Strained flamelets for turbulent premixed flames II: laboratory flame results. Combust Flame 2010;157:1274–89.

[63] Darbyshire OR, Swaminathan N, Hochgreb S. The effects of small-scale mixing models on the prediction of turbulent premixed and stratified combustion. Combust Sci Technol 2010;182:1141–70.

[64] Hernández-Pérez F, Yuen F, Groth C, Gülder Ö. LES of a laboratory-scale turbulent premixed Bunsen flame using FSD, PCM-FPI and thickened flame models. Proc Combust Inst 2011;33:1365–71.

[65] Darbyshire OR, Swaminathan N. A presumed joint PDF model for turbulent combustion with varying equivalence ratio. Combust Sci Technol 2012;184:2036–67.

[66] Salehi MM, Bushe WK, Shahbazian N, Groth CRT. Modified laminar flamelet presumed probability density function for LES of premixed turbulent combustion. Proc Combust Inst 2013;34:1203–11.

[67] Klapdor EV, di Mare F, Kollmann W, Janicka J. A compressible pressure-based solution algorithm for gas turbine combustion chambers using the PDF/FGM model. Flow, Turbul Combust 2013;191:209–47.

[68] Trisjono P, Kleinheinz K, Kang S, Pitsch H. Large eddy simulation of stratified and sheared flames of a premixed turbulent stratified flame burner using a flamelet model with heat loss. Flow, Turbul Combust 2014;92:201–35.

[69] Hernández-Pérez F, Groth C, Gülder Ö. Large-eddy simulation of lean hydrogen-methane turbulent premixed flames in the methane-dominated regime. Int J Hydrogen Energy 2014;39:7147–57.

[70] Nambully S, Domingo P, Moreau V, Vervisch L. A filtered-laminar-flame PDF sub-grid scale closure for LES of premixed turbulent flames: I. Formalism and application to a bluff-body burner with differential diffusion. Combust Flame 2014;161:1756–74.

[71] Nambully S, Domingo P, Moreau V, Vervisch L. A filtered-laminar-flame PDF sub-grid scale closure for LES of premixed turbulent flames: II. Application to a stratified bluff-body burner. Combust Flame 2014;161:1775–91.

[72] Donini A, Bastiaans RJM, van Oijen JA, Day MS, de Goey LPH. An a priori DNS subgrid analysis of the presumed β-PDF model. Int J Hydrogen Energy 2015;40:12811–23.

[73] Shahbazian N, Salehi MM, Groth CPT, Gülder ÖL, Bushe WK. Performance of conditional source-term estimation model for LES of turbulent premixed flames in thin reaction zones regime. Proc Combust Inst 2015;35(2):1367–75.

[74] van Oijen JA, Donini A, Bastiaans RJM, ten Thije Boonkkamp JHM, de Goey LPH. State-of-the-art in premixed combustion modeling using flamelet generated manifolds. Prog Energy Combust Sci 2016;57:30–74.

[75] Langella I, Swaminathan N. Unstrained and strained flamelets for LES of premixed combustion. Combust Theor Model 2016;20:410–40.

[76] Langella I, Swaminathan N, Pitz RW. Application of unstrained flamelet SGS closure for multiregime premixed combustion. Combust Flame 2016;173:161–78.

[77] Ottino GM, Fancello A, Falcone M, Bastiaans RJM, de Goey LPH. Combustion modeling including heat loss using Flamelet Generated Manifolds: a validation study in OpenFOAM. Flow, Turbul Combust 2016;96:773–800.

[78] Dovizo D, Debbagh A, Devaud CB. RANS simulations of a series of turbulent V-shaped flames using conditional source-term evaluation. Flow, Turbul Combust 2016;96:891–919.

[79] Lapointe S, Blanquart G. A priori filtered chemical source term modeling for LES of high Karlovitz number premixed flames. Combust Flame 2017;176:500–10.

[80] Donini A, Bastiaans RJM, van Oijen JA, de Goey LPH. A 5-D implementation of FGM for the large eddy simulation of a stratified swirled flame with heat loss in a gas turbine combustor. Flow, Turbul Combust 2017;98:887–922.

[81] Galeazzo FCC, Savard B, Wang H, Hawkes ER, Chen JH, Filho GCK. Performance assessment of flamelet models in flame-resolved LES of a high Karlovitz methane/air stratified premixed jet flame. Proc Combust Inst 2019;37:2545–53.

[82] Nilsson T, Yu R, Doan NAK, Langella I, Swaminathan N, Bai X. Filtered reaction rate modelling in moderate and high Karlovitz number flames: an a priori analysis. Flow, Turbul Combust 2019;103:643–65.

[83] Sabelnikov VA, Yu R, Lipatnikov AN. Thin reaction zones in constant-density turbulent flows at low Damköhler numbers: theory and simulations. Phys Fluids 2019;31:055104.

[84] Driscoll JF, Chen JH, Skiba AW, Carter CD, Hawkes ER, Wang H. Premixed flames subjected to extreme turbulence: some questions and recent answers. Prog Energy Combust Sci 2020;76:100802.

[85] Gicquel O, Darabiha N, Thévenin D. Laminar premixed hydrogen/air counterflow flame simulations using flame prolongation of ILDM with differential diffusion. Proc Combust Inst 2000;28:1901–8.

[86] van Oijen JA, de Goey LPH. Modeling of premixed laminar flames using flamelet generated manifolds. Combust Sci Technol 2000;161:113–37.

[87] Lipatnikov AN. Stratified turbulent flames: recent advances in understanding the influence of mixture inhomogeneities on premixed combustion and modeling challenges. Prog Energy Combust Sci 2017;62:87–132.

[88] Lipatnikov AN. Fundamentals of premixed turbulent combustion. CRC Press; 2012.

[89] Peters N. Turbulent combustion. Cambridge University Press; 2000.

[90] Lipatnikov AN, Chomiak J. Effects of premixed flames on turbulence and turbulent scalar transport. Prog Energy Combust Sci 2010;36(1):1–102.

[91] Sabelnikov VA, Lipatnikov AN. Recent advances in understanding of thermal expansion effects in premixed turbulent flames. Annu Rev Fluid Mech 2017;49:91–117.

[92] Dave H, Chaudhuri S. Evolution of local flame displacement speeds in turbulence. J Fluid Mech 2020;884:A46.

[93] Babkovskaia N, Haugen NEL, Brandenburg A. A high-order public domain code for direct numerical simulations of turbulent combustion. J Comput Phys 2011;230(1):1–12.

[94] Dave HL, Mohan A, Chaudhuri S. Genesis and evolution of premixed flames in turbulence. Combust Flame 2018;196:386–99.

[95] Poinsot TJ, Lele SK. Boundary conditions for direct simulations of compressible viscous flows. J Comput Phys 1992;101:104–29.

[96] Li J, Zhao Z, Kazakov A, Dryer FL. An updated comprehensive kinetic model of hydrogen combustion. Int J Chem Kinet 2004;36(10):566–75.

[97] Kuron M, Hawkes ER, Ren Z, Tang JCK, Zhou H, Chen JH, Lu T. Performance of transported PDF mixing models in a turbulent premixed flame. Proc Combust Inst 2017;36(1):1987–95.

[98] Lipatnikov AN, Chomiak J. Turbulent flame speed and thickness: phenomenology, evaluation, and application in multi-dimensional simulations. Prog Energy Combust Sci 2002;28(1):1–73.

[99] Poinsot T, Veynante D. Theoretical and numerical combustion. Edwards. 2nd ed. 2005.

[100] Bilger RW, Pope SB, Bray KNC, Driscoll JF. Paradigms in turbulent combustion research. Proc Combust Inst 2005;30(1):21–42.

[101] Echekki T, Mastorakos E, editors. Turbulent combustion modeling. Springer; 2011.

[102] Swaminathan N, Bray KNC, editors. Turbulent premixed flames. Cambridge University Press; 2011.

[103] Prudnikov AG. In: Raushenbakh VB, editor. Physical principles of the working process in combustion chambers of jet engines. Clearing House for Federal Scientific & Technical Information; 1967. p. 244–336.

[104] Tamadonfar P, Gülder ÖL. Flame brush characteristics and burning velocities of premixed turbulent methane/air Bunsen flames. Combust Flame 2014;161:3154–65.

[105] Han D, Satija A, Gore JP, Lucht RP. Experimental study of CO_2 diluted, piloted, turbulent CH_4/air premixed flames using high-repetition-rate OH PLIF. Combust Flame 2018;193:145–56.

[106] Lipatnikov AN, Chomiak J. A theoretical study of premixed turbulent flame development. Proc Combust Inst 2005;30(1):843–50.

[107] Lipatnikov AN, Chomiak J. Self-similarly developing, premixed, turbulent flames: a theoretical study. Phys Fluids 2005;17:065105.

[108] Lipatnikov AN. In: De S, Agarwal AK, Chaudhuri S, Sen S, editors. Modeling and simulation of turbulent combustion. Springer Nature Singapore Pte Ltd; 2018. p. 181–240.

[109] Karlovitz B, Denniston DW, Wells FE. Investigation of turbulent flames. J Chem Phys 1951;19:541–7.

[110] Sponfeldner T, Soulopoulos N, Beyrau F, Hardalupas Y, Taylor AMKP, Vassilicos JC. The structure of turbulent flames in fractal- and regular-grid-generated turbulence. Combust Flame 2015;162:3379–93.

[111] Lapointe S, Blanquart G. Fuel and chemistry effects in high Karlovitz premixed turbulent flames. Combust Flame 2016;167:294–307.

[112] Wang Z, Magi V, Abraham J. Turbulent flame speed dependencies of lean methane-air mixtures under engine relevant conditions. Combust Flame 2017;180(1):53–62.

[113] Bray KNC, Libby PA, Moss JB. Unified modeling approach for premixed turbulent combustion - Part I: general formulation. Combust Flame 1985;61(1):87–102.

[114] Lipatnikov AN, Nishiki S, Hasegawa T. A modified presumed PDF approach to modeling premixed turbulent flames. In: Selçuk N, Beretta F, Mansour MS, D'Anna A, editors. Proceedings of the eighth mediterranean combustion symposium; September 8-13 2013 [Çeşme, Izmir, Turkey].

[115] Kuznetsov VR, Sabelnikov VA. Turbulence and combustion. Hemisphere; 1990.

[116] Kaskan WE. The concentration of hydroxyl and of oxygen atoms in gases from lean hydrogen-air flames. Combust Flame 1958;2(3):286–304.

[117] Williams FA. Progress in knowledge of flamelet structure and extinction. Prog Energy Combust Sci 2000;26:657–82.